


Investigation of anisotropy in the collective dynamics and thermal diffusivity in the phenyl pyrimidine liquid crystal

Meguya Ryu National Metrology Institute of Japan (NMIJ), *National Institute of Advanced Industrial Science and Technology (AIST)*, Tsukuba 305-8563, Japan

Shu-hei Kurose

School of Materials and Chemical Technology, *Institute of Science Tokyo (Science Tokyo)*, Meguro-ku, Tokyo 152-8550, JapanKoji Yoshida Department of Chemistry, Faculty of Science, *Fukuoka University*, Fukuoka 814-0180, JapanHiroshi Uchiyama *Japan Synchrotron Radiation Research Institute*, SPring-8, Sayo, Hyogo 679-5198, JapanJunko Morikawa *School of Materials and Chemical Technology, Meguro-ku, Tokyo 152-8550, Japan
and Research Center for Autonomous Systems Materialogy (ASMat), Institute of Integrated Research (IIR),
Institute of Science Tokyo (Science Tokyo), Yokohama 226-8501, Japan

(Received 17 September 2024; accepted 17 December 2024; published 28 January 2025)

Liquid crystals (LCs) are unique heat transfer media that exhibit large anisotropy in thermal properties depending on the direction of the director (n) of the LC state. This phenomenon is the basis of thermal conduction in ordered soft materials, and has been extensively studied to understand thermal conduction in soft materials. In this study, we used inelastic x-ray scattering (IXS) to investigate the anisotropic thermal diffusivity and collective dynamics in the terahertz region of a pyrimidine-type LC (PYP8O8). The dispersion relations at several frequencies corresponding to the LC state were analyzed in the directions parallel and perpendicular to n . The results showed that there was a significant difference between the anisotropy of the sound velocity and that of the attenuation coefficient (Γ) estimated from the shape parameter of the IXS spectrum. The results for the linewidth of inelastic excitation show Q^2 dependence that is far beyond the viscoelastic relaxation of the system, and the anisotropy in the collective dynamics predicted by Forster *et al.* [*Phys. Rev. Lett.* **26**, 1016 (1971)] in the hydrodynamic region can be extensively applied to the more localized collective motion of LC systems.

DOI: [10.1103/PhysRevE.111.015432](https://doi.org/10.1103/PhysRevE.111.015432)

I. INTRODUCTION

One of the prominent characteristics of soft materials is the anisotropy in their transportation properties such as thermophysical properties. Phonons are fundamental processes in the directional transport of sound and heat [1]. Studying the dispersion of phonons leads to an understanding of thermal diffusion, especially its anisotropy, in materials [2]. The anisotropy of thermophysical properties in soft materials is attracting attention as dynamically controllable heat

transport media [3]. Liquid crystals (LCs) are the basic systems of soft materials, and their applications in controlling the anisotropies of thermophysical properties have been actively investigated [4,5].

Since soft materials are composed of individual molecules, their properties are highly dependent on their higher-order structure in multiple scales, and their bulk properties are produced from the static structure and the collective dynamics of the molecules [6]. Therefore, investigating the relationship between the bulk properties, such as thermophysical properties, and the static structure and collective dynamics, is important for the development of advanced materials from a phonon engineering perspective.

The correlation between the thermophysical anisotropy and the long-wavelength group dynamics in liquid crystalline systems has been investigated by Brillouin light scattering (BLS) and temperature wave analysis (TWA) [7]. BLS and TWA analysis of the liquid crystalline phase of a phenylpyrimidine-type molecule (PYP8O8) revealed that the anisotropy in the

*Contact author: morikawa.j.aa@m.titech.ac.jp, morikawa.j.4f50@m.isct.ac.jp

Published by the American Physical Society under the terms of the [Creative Commons Attribution 4.0 International](https://creativecommons.org/licenses/by/4.0/) license. Further distribution of this work must maintain attribution to the author(s) and the published article's title, journal citation, and DOI.

thermal diffusivity (D_T) and the hydrodynamic sound velocity (c_0) had clear differences. The anisotropy in D_T is mostly correlated with the order parameter S through the following equation [4]:

$$\frac{D_{T\parallel}}{D_{T\perp}} = \frac{D_{T\parallel}^*(1-S) + D_{T\perp}^*(2+S)}{D_{T\parallel}^*(1+2S) + D_{T\perp}^*(2-2S)}, \quad (1)$$

where $D_{T\parallel}$ is the thermal diffusivity along n , $D_{T\perp}$ is the thermal diffusivity normal to n , $D_{T\parallel}^*$ is the thermal diffusivity along an individual molecular axis, $D_{T\perp}^*$ is that of normal to it, while there are very small anisotropies in the hydrodynamic sound velocity (c_0) measured by BLS. This result has also been confirmed in liquid crystalline elastomer systems, where the contribution of anisotropy in c_0 is higher than in the case of LC; however, it is still smaller than the anisotropy in the thermophysical properties. The increase of the anisotropy in c_0 can be explained by an increase in the interactions between individual molecules [8].

Previous studies for LCs have investigated phonons in the long-wavelength region (gigahertz range) [7,9]; however, the anisotropy of dynamics in smaller scales is not yet clear. The wavelength of the probing elastic wave is above 100 nm, which corresponds to the size of molecular clusters. The phonon scales investigated by inelastic x-ray scattering (IXS) are around a few angstrom, which is the scale of a single molecule. The recent investigation of a LC system by all-atom molecular dynamics reported that the anisotropy of heat diffusion in a LC system is strongly affected by the directional intermolecular interaction [10], so that the molecular scale dynamics in a LC system may play an important role in the thermal diffusion in the system.

Investigations of collective dynamics using IXS have been performed to develop a highly efficient heat transfer medium [11]. Therefore, investigations of anisotropy in the collective dynamics of a LC system using IXS may also accelerate our understanding of anisotropic thermal diffusion in such systems. IXS has recently been used to investigate phonon dispersion relationships in soft materials such as liquid crystals and lipids, but the anisotropic phonon group velocity has not yet been investigated, and this could provide insight into the origin of anisotropic thermal diffusion [12,13].

In this study, the collective dynamics of LC was measured by IXS experiments along two different directions of the transfer momentum (Q) in an ordered LC system (i.e., two measurement configurations of $Q \perp n$ and $Q \parallel n$ were realized) and the measurement was performed at a different phase of LC. The obtained dispersion of the energy and the sound velocity is discussed according to the hydrodynamics theory of a LC system. The results of anisotropy are also compared with the previous investigation by using a BLS technique, which has strongly reduced spectral resolution in the gigahertz region (FWHM $\approx 10^{-3}$ meV) [7].

II. EXPERIMENT

A. Inelastic x-ray scattering

IXS experiments with a high intensity and high linearly x-ray from synchrotron radiation were carried out at the IXS beamline (BL35XU) in SPring-8. Incident x-rays are

monochromatized at 21.75 keV with a resolution of 1.5 meV mainly achieved by two monochromators—a Si(1 1 1) high heat-load monochromator and a Si(11 11 11) back scattering monochromator. Monochromatized x-rays were then incident on the sample and the scattered beam at the selected angle was analyzed by the 10 m arm of the analyzer. The momentum transfer Q value is scanned by changing the angle of the arm. The x-ray energy can be scanned by changing the spacing of the crystal lattice by varying the temperature of the backscattering monochromator. The above two parameters can then be scanned to obtain the dispersion relation between energy and momentum. The incident x-ray energy was scanned ± 20 meV and the momentum transfer (Q) from 1.14 to 11.14 nm $^{-1}$.

B. Liquid crystal sample for in-plane scattering

In this study, LC samples were kept between two glass substrates of a sample cell to obtain the uniaxial alignment by the surfactant (alignment layer). However, LCs are soft materials composed mainly of carbon and hydrogen and have a low scattering cross section to x-rays, so thick samples, e.g., millimeter scale, are needed to obtain sufficient inelastic scattering signals from them. Therefore, an x-ray for IXS measurement was irradiated along the in-plane direction of the film-shaped LC sample.

A schematic of the LC sample cell used in the IXS experiment is shown in Fig. 1(a). The LC sample was inserted between two glass substrates (0.7 mm thickness) and a Kapton film spacer was used to keep the gap between the substrates at about 200 μ m. The horizontal length (y direction) of the cell is 30 mm and the vertical (x direction) length is 5 mm. Then, x-rays with a diameter of 100 μ m are transmitted along the in-plane direction of the LC film almost along the x direction. As a result, the Q vector is parallel to y and the scattering in the x - y plane is measured.

LC molecules were aligned along a specific direction in the sample cell. The molecules were oriented in the x - y plane in the cell using a polyimide-type surfactant layer (AL 1254). The orientation direction of a LC molecule was controlled by a rubbing direction R . In this experiment, two types of cells with two different directions of rubbing ($R \parallel x$ and $R \parallel y$) were prepared and realized $Q \perp n$ [Fig. 1(b1)] and $Q \parallel n$ [Fig. 1(b2)] configurations. The irradiation position of incident x-ray was scanned along the y direction during IXS measurement to avoid degradation of the sample.

A typical LC molecule of 5-*n*-octyl-2-(4-*n*-octyloxyphenyl)-pyrimidine (PYP8O8; C₂₆H₄₀N₂O) was chosen for LC samples in this study. This LC molecule has side chains with eight carbon atoms on either side of a rigid phenyl pyrimidine core. As temperature increases, the LC sample has the following phase sequence: Crys-29-SmC-56-SmA-62-N-69-Iso, where the numbers indicate the transition temperatures (in degrees Celsius) between the adjacent LC phases (Crys: crystalline solid; SmC: smectic-C LC; SmA: smectic-A LC; N: nematic LC; and Iso: isotropic liquid). IXS experiments were performed at fixed sample temperatures for each LC phase. PYP8O8 was chosen because it exhibits five well-separated phases in a manageable temperature range (e.g., 20 °C–90 °C).

For the temperature variable IXS experiment, a home-made temperature-controllable chamber was designed. A

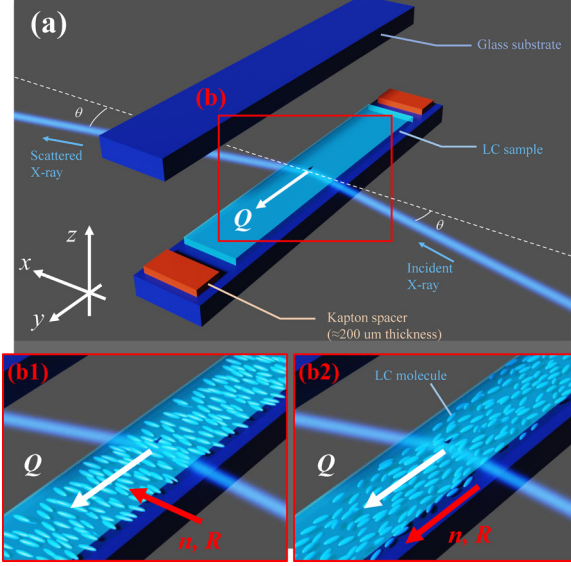


FIG. 1. (a) The schematic view of the LC sample used for the IXS experiment. The sample LC is inserted between two 700- μm -thick glass substrates. The gap between the substrates is 200 μm and it is held by the 200- μm -thick Kapton spacer. The sample cell is the rectangular shape having a lateral (y direction in the figure) length of 30 mm and a vertical (x direction) length of 5 mm. The Q vector is aligned parallel to the lateral direction and the scattering plane is horizontal to the sample cell (the x - y plane). The incident x-ray having 100 μm diameter is the path through the gap between the substrates. The detailed schematic of region (b) is depicted in (b1) and (b2). Two types of LC cells were prepared with two different directions of rubbing processes (R), which result in two different directions of LC molecule directors (n) in LC phase parallel to R . The two types of cells effectively achieve (b1) $Q \perp n$ and (b2) $Q \parallel n$ configurations.

sheet heater was mounted inside a block of copper, on which the sample was fixed. The heater was covered by an aluminum outer shell. The chamber was filled with helium (He) gas to reduce the scattering from the atmosphere, and x-rays were transmitted through the slit on the chamber wall fitted with Kapton windows of thickness 7 μm .

III. RESULTS AND DISCUSSION

A. IXS spectra at different LC states

The measured IXS spectra shows quasielastic Lorentzian peaks at central position, and Stokes and anti-Stokes peaks of the dispersive acoustic mode. The experimental data of IXS is analyzed by using a Lorentzian and a damped harmonic oscillator (L + DHO) model. The triplet feature of this spectrum can be described by the dynamic structure factor $S(Q, \omega)$ in the following form [14]:

$$S(Q, \omega) = \frac{S(Q)}{\pi} \left[A_0 \frac{\Gamma_0}{\omega^2 + \Gamma_0^2} + A_1 \frac{2\Gamma_1\omega_1^2}{(\omega^2 - \omega_1^2)^2 + 4\omega^2\Gamma_1^2} \right], \quad (2)$$

where ω is the frequency, A_0 and Γ_0 are the intensity and width (damping factor) of the central quasielastic peak, A_1 and Γ_1 are those for the inelastic peak, and ω_1 is the energy of the

sound mode, respectively. $S(Q)$ is the static structure factor calculated by integrating the spectral intensity over the whole energy range of measurement (from -20 meV to $+20$ meV).

Scattering intensity data $I(Q, \omega)$ was analyzed by the dynamic structure factor in Eq. (2) convoluted with the experimentally measured energy dispersion of the incident beam [resolution function, $R(\omega)$], and Bose factor $B(\omega)$ as follows [15]:

$$I(Q, \omega) = \frac{1}{S(Q)} \int B(\omega') S(Q, \omega') R(\omega - \omega') d\omega. \quad (3)$$

The resolution function was estimated from the measurement of polymethyl methacrylate, which exhibits the elastic scattering only. The measured resolution function was fitted by the pseudo-Voigt function, which is a multiplication of the Lorentzian and Gaussian shape functions. The function can be written as follows [16]:

$$R(\omega) = \frac{AM}{1 + 4(\omega/\Gamma_L)^2} + A(1 - M) \exp\{-4 \ln 2(\omega/\Gamma_G)^2\}, \quad (4)$$

where A is the intensity of the peak, M is the mixing parameter of two functions, and Γ_L and the Γ_G are the FWHM of the Lorentzian and Gaussian peaks, respectively [14].

The Bose factor $B(\omega)$ is an asymmetrical weight factor in the Stokes and anti-Stokes regimes, known to depend on temperature and described as follows [17]:

$$B(\omega) = \frac{\hbar\omega/k_B T}{1 - \exp(-\hbar\omega/k_B T)}, \quad (5)$$

where \hbar , k_B , and T are the Dirac constant, the Boltzmann constant, and temperature, respectively. The raw IXS spectra and fitted curves of the N, SmA, and SmC phases of PYP8O8 in different aligned directions are shown in Fig. 2 as examples of spectra data. The blue dots are the raw data obtained from the energy scan of the IXS experiment and the red line is the total fitting function $I(Q, \omega)$ expressed in Eq. (3). The dark line is the inelastic components $S(Q, \omega)$ in the total fitting function as expressed in Eq. (2). The dashed line corresponds to the resolution function $R(\omega)$, independent on Q and dependent on the sensor of the measuring instrument.

B. Static structure factor

The Q dependency of $S(Q)$ was firstly checked to confirm the experimental configuration and LC alignment. Figure 3 shows $S(Q)$ at different temperatures along two different directions ($Q \perp n$ and $Q \parallel n$) of LC system. At all temperatures $S(Q)$ shows peak at around 2.47 nm^{-1} for the $Q \parallel n$ direction, which corresponds to the length of the LC molecule ($L_{\parallel} \approx 25.2 \text{ \AA}$). At the high- Q region, $S(Q)$ of the $Q \perp n$ configuration always shows a higher intensity, which reflects the scattering halo expected around 14 nm^{-1} corresponding to the intermolecular distance ($L_{\perp} \approx 5 \text{ \AA}$) between LC molecules. The $S(Q)$ data confirm that our experiments were successfully conducted along $Q \perp n$ and $Q \parallel n$. The schematics of the LC system and the definition of the characteristic length are shown in Fig. 8 in Appendix A.

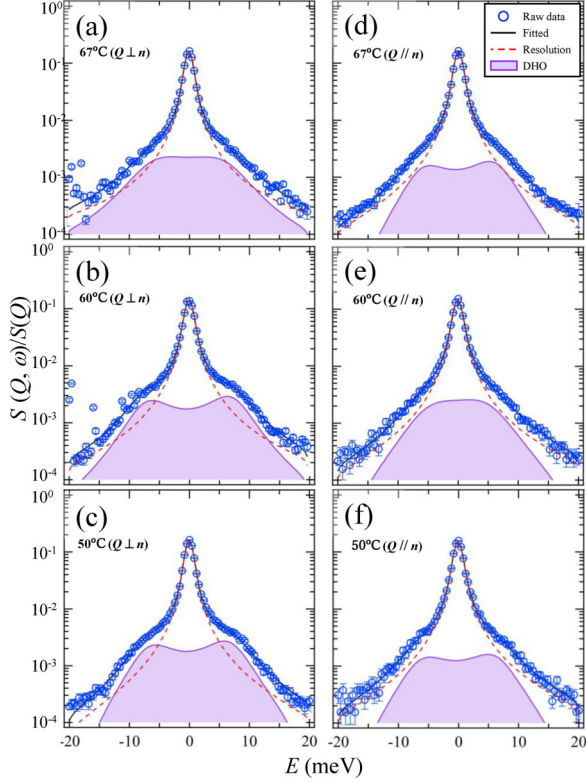


FIG. 2. IXS spectra $S(Q, \omega)/S(Q)$ of N [(a),(d), 67°C], SmA [(b),(e), 60°C], and SmC [(c),(f), 50°C] phases of PYP8O8 in two different orientations measured at $Q = 6.24 \text{ nm}^{-1}$. The raw spectra were deconvoluted by the resolution function of the incident x-ray (dashed red line) and the inelastic peak was determined. Blue points are raw data, the black solid line is the fitting curve, and the purple filled area plot is the inelastic component. (a)–(c) The IXS spectra measured with configurations of $Q \perp n$ and (d)–(f) $Q \parallel n$.

C. Dispersion curves

The inelastic peak position was determined from the fitting parameter (ω_1) in Eq. (2). The analysis was performed for all spectra at different Q and for the data taken with the configurations of $Q \perp n$ and $Q \parallel n$. Figure 4 shows the dispersion relation between ω_1 and Q for the N, SmA, and SmC phases of PYP8O8. Blue points [Figs. 4(a)–4(c)] correspond to $Q \perp n$, and the red points [Figs. 4(d)–4(f)] correspond to $Q \parallel n$, respectively. The dashed line replots the dispersion relation measured by BLS, where the slope corresponds to the hydrodynamic sound velocity [7]. In the following discussion, the measured Q range is divided into three regions, namely, (i) $Q < 3 \text{ nm}^{-1}$, (ii) $3 \text{ nm}^{-1} < Q < 7 \text{ nm}^{-1}$, and (iii) $Q > 7 \text{ nm}^{-1}$. The acoustic mode in region (i) follows the dispersion observed by BLS; however, it disperses with the velocity higher than the hydrodynamic sound velocity (positive dispersion) in region (ii).

The dispersion relationships of energies measured in the IXS experiments are also similar in the two directions, $Q \perp n$ and $Q \parallel n$. In Q region (iii), a decrease of energy dispersion with increasing Q is observed that mainly corresponds to the

strong scattering of collective excitation on the cage of nearby molecules. This phenomena is commonly observed upon approaching the first diffraction peak, which corresponds to the intermolecular distance in the case of molecular liquid [18]. The maximum energy is observed in region (iii) that corresponds to the length scale smaller than 0.90 nm ($L = 2\pi/Q$) in the case of $Q \perp n$ [Figs. 4(a)–4(c)], which is the scale comparable to L_\perp .

It is also expected to observe the maximum of excitation energy at smaller Q values in region (iii) for the $Q \parallel n$ measurement due to longer structural periodicity [Figs. 4(d)–4(f)]; however, it is difficult to distinguish the peak position due to the large uncertainty of estimated ω_1 values in region (iii). It should also be noted that the sudden increase of uncertainty (low signal-to-noise ratio) in ω_1 (i.e., reduction in intensity of inelastic peak) is observed in region (iii), which may be related to the strong dumping of collective motion emerging from this region. In $S(Q)$ of the $Q \parallel n$ configuration, the scattering intensity gradually increased in region (iii).

The above-mentioned scattering effect appears at a higher Q value in region (iii) in the case of $Q \parallel n$ at 67°C [Fig. 4(d)], compared to 50°C [Fig. 4(f)]. The order parameter (f) of LC usually decreases with increasing temperature towards T_{NI} where f becomes 0 at the isotropic phase. Therefore, the decrease of the average intermolecular distance along $Q \parallel n$ due to the decrease of f can be the reason for the shift of the starting Q position of large scattering towards the high- Q direction with increasing temperature. It can also be seen that an extremely large uncertainty of ω_1 was observed in region (i) of the $Q \parallel n$ measurements. This can be considered as large elastic scattering corresponds to the formation of the layered structure in the smectic phase, which has about 30 Å ($\approx 2.09 \text{ nm}^{-1}$) layer spacing [19–21].

The dispersion of dynamic sound (DS) speed $c(Q) = \omega_1/Q$ for each LC phase is shown in Fig. 5 for two directions of LC molecules. The dashed line of c_0 indicates the hydrodynamic sound velocity measured by BLS, and c_∞ indicates the maximum DS speed estimated from the plot. The high-frequency sound velocity c_∞ is almost 30% higher than the hydrodynamic sound velocity c_0 for all samples, decreasing with increasing temperature, similar to the temperature dependency of c_0 . The increase in the speed of sound from c_0 to c_∞ is observed as structural relaxation such as in the glass (α) relaxation process in glass-forming systems, which causes the liquid glass transition in systems that can maintain strong supercooling.

The anisotropy of c_∞ and c_0 is different, with c_∞ being almost isotropic within the range of analytical uncertainty between the directions of $Q \parallel n$ and $Q \perp n$. On the other hand, c_0 shows a higher sound velocity along the direction of $Q \parallel n$. Consequently, the rate at which the sound velocity increases from c_0 to c_∞ differs between $Q \perp n$ and $Q \parallel n$. The dispersion of the sound velocity exhibits a typical tendency of positive dispersion. Although the previous BLS study of region (i) observed the anisotropy corresponding to region (i) [7], the anisotropy between the two directions of $Q \perp n$ and $Q \parallel n$ is negligible in the dispersion relationship in regions (ii) and (iii) in this study.

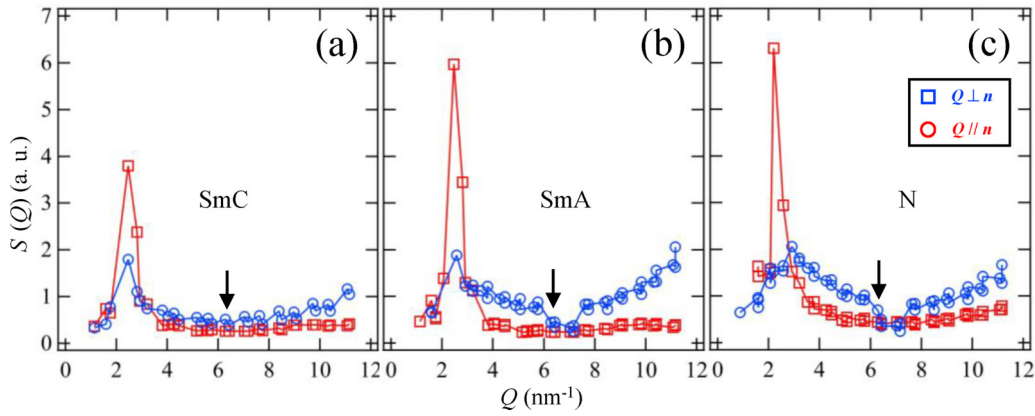


FIG. 3. The static structure factor $S(Q)$ for different LC phases. (a) SmC phase at 50 °C, (b) SmA phase at 60 °C, and (c) N phase at 67 °C. The data point with the blue open square corresponds to the experiments with $Q \perp n$ configuration and the open red circle corresponds to the $Q \parallel n$ configuration. The arrow indicates the position where the spectra in Fig. 2 were measured. For the schematics of the LC system and the definition of the characteristic length, see Fig. 8 in Appendix A.

D. Anisotropy

Figure 6 shows Q dependency of HWHM of the inelastic peak (Γ_1) measured at different LC phases with $Q \parallel n$ and $Q \perp n$ configurations. It should be noted that the dispersion well follows Q^2 dependency even beyond the viscoelastic

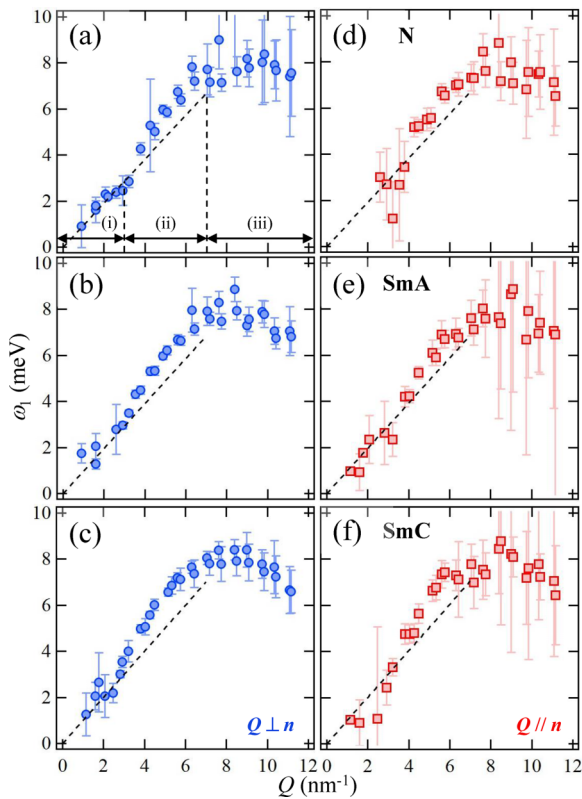


FIG. 4. The dispersion relationship of PYP8O8 along the molecular axis ($Q \parallel n$) (a)–(c) and along the perpendicular direction to the molecular axis ($Q \perp n$) (d)–(f). The measurement was performed at (a), (d) 67 °C in the N phase, (b), (e) 60 °C in the SmA phase, and (c), (f) 50 °C in the SmC phase, respectively. The error bars correspond to the 95% confidential region of the analysis. The black dashed lines are the measured results in Ref. [7].

transition observed in the dispersion of sound velocity [from Q region (i) to (ii)]. In the case of dispersion of Γ_1 , there are

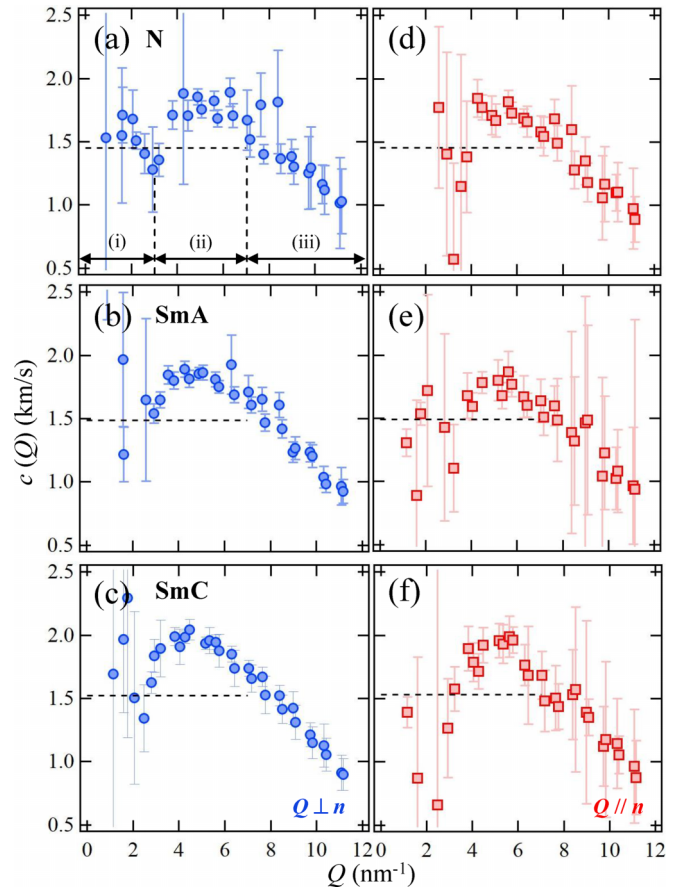


FIG. 5. The Q dependency of the dynamic sound (DS) speed $c(Q) = \omega_1/Q$ of PYP8O8 along the molecular axis ($Q \parallel n$) (a)–(c) and along the perpendicular direction to the molecular axis ($Q \perp n$) (d)–(f). The measurement was performed at (a), (d) 67 °C in the N phase, (b), (e) 60 °C in the SmA phase, and (c), (f) 50 °C in the SmC phase, respectively. Horizontal dashed lines indicate the hydrodynamic sound speed (c_0) measured by BLS. The high-frequency sound velocity (c_∞) was estimated from the maximum value of the DS speed appearing at around 4 nm⁻¹.

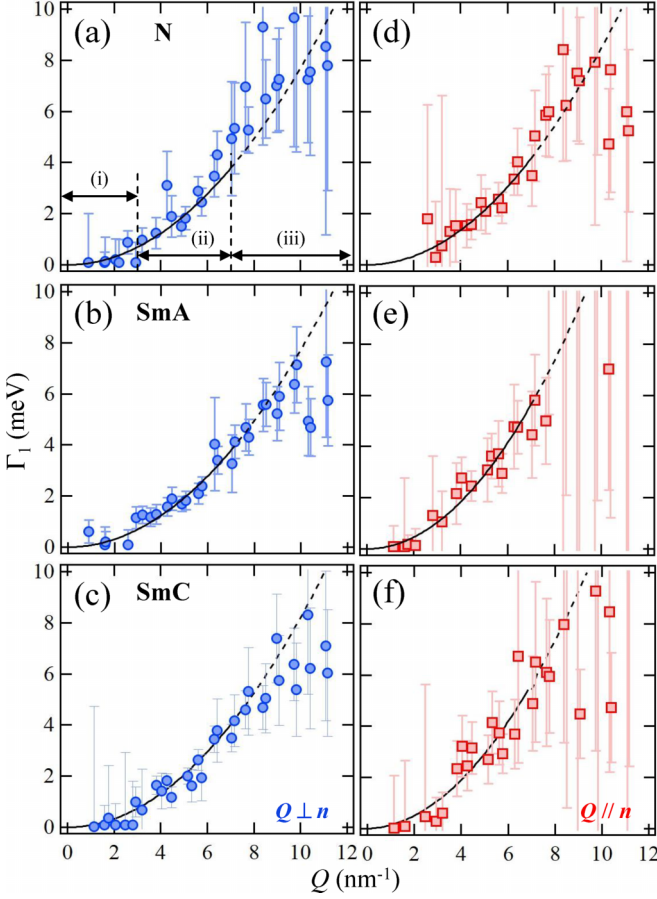


FIG. 6. The Q dependency of the HWHM of inelastic peak (Γ_1) of PYP808 along the molecular axis ($Q \parallel n$) (a)–(c) and along the perpendicular direction to the molecular axis ($Q \perp n$) (d)–(f). The measurement was performed at (a), (d) 67 °C in the N phase, (b), (e) 60 °C in the SmA phase, and (c), (f) 50 °C in the SmC phase, respectively. The dashed line corresponds to the best fit to Q^2 dependencies analyzed by data points in Q regions (i) and (ii) where hydrodynamic asymptotic is applicable. See the logarithmic plot of Γ_1 vs Q in Fig. 9 in Appendix B.

significant differences between the $Q \parallel n$ and $Q \perp n$ configurations. Γ_1 along the $Q \parallel n$ direction is always larger than that of the $Q \perp n$ direction, suggesting smaller attenuation of the propagating sound wave along the molecular axis direction ($Q \parallel n$). To analyze the difference of Q^2 dependency of Γ_1 along two directions, the data were fitted by the equation $\Gamma_1 = \Gamma Q^2$. Here, the constant Γ is the sound attenuation constant.

Figure 7(a) shows the temperature dependence of c_∞ from IXS measurements along $Q \parallel n$ and $Q \perp n$ and Fig. 7(b) shows the temperature dependence of Γ along two directions. The error bar of the plot denotes a 95% confidential region of each analysis. It can be seen that the sound attenuation Γ has a clear anisotropy in the LC state, while c_∞ is almost isotropic at the entire temperature range of the measurement. For the measurement at nematic state (67 °C), the anisotropy of Γ is decreasing compared to other temperatures. This can be considered as the effect of order parameter f , which decreases when the transition temperature between isotropic liquid and nematic (T_{NI}) is approaching. The anisotropy in Γ observed

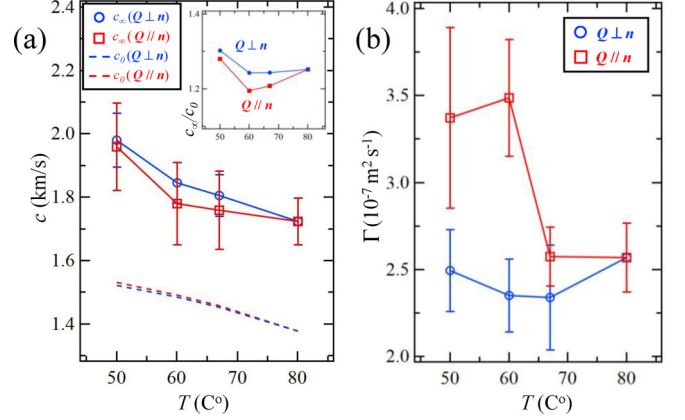


FIG. 7. (a) Temperature dependency of high-frequency sound velocity c_∞ from IXS (markers with lines) and the hydrodynamic sound velocity c_0 from BLS (dashed lines) measurements along two directions of $Q \perp n$ (blue open circle) and $Q \parallel n$ (red open square). Inset: Temperature dependency of c_∞/c_0 . (b) Temperature dependency of the sound attenuation coefficient estimated from the dispersion curve of Γ_1 . The values along the two directions of $Q \perp n$ (blue open circle) and $Q \parallel n$ (red open square) are compared.

in this study is at around 1.5 times the maximum, which is still smaller than that observed in thermal diffusivity. The anisotropy of thermal diffusivity ($D_{T\perp}/D_{T\parallel}$) measured by TWA was between 2 and 3 for PYP808 in the LC phase [7]. The temperature dependency of c_0 along two different directions and the temperature dependency of the ratio c_∞/c_0 are also plotted in Fig. 7(a), showing that the anisotropies appear differently in c_0 and c_∞ , and the amplitude of structural relaxation is also anisotropic.

The phonon attenuation in the material and its anisotropy is an important characteristic of a LC system where viscosity constant is associated with Γ_1 as $\eta = \frac{2\pi\rho}{Q^2} \Gamma_1$. Here, ρ is the bulk density which can be considered as an isotropic property. It has been predicted that in the framework of hydrodynamics, the characteristics of angular dependency to the molecular direction only appear in the sound attenuation and the thermal diffusivity [22], and the anisotropic sound attenuation coefficient (Γ) is constructed with five independent components of viscosity tensor η_{ij} as follows.

$$\Gamma = \frac{1}{2\pi\rho} \{ \eta_{11} \sin^2 \phi + \eta_{33} \cos^2 \phi + (2\eta_{13} + 4\eta_{44} - \eta_{11} - \eta_{33}) \sin^2 \phi \cos^2 \phi \}. \quad (6)$$

Here, ϕ is the angle between n and Q .

This prediction has been observed in the collective dynamics measured by a light-scattering technique; however, the hydrodynamic picture of LC is also applicable for the results shown in this study measured in the terahertz range. We also observed the positive dispersion of dynamic sound velocity that may be related to the certain structural relaxation process. Some characteristics of hydrodynamic anisotropies remain even after the viscoelastic transition (liquidlike to solidlike transition) of LC.

The anisotropy in the sound attenuation is also more pronounced than that in the sound velocity, even in the gighertz

region measured by BLS for LC elastomers [8]. It suggests that the viscosity has a greater sensitivity to the anisotropy of the LC system than elasticity. The measurement of this study shows that the description of a LC system using the hydrodynamic model in the previous study [22] can be further applicable to the terahertz range dynamics. The LC system investigated in this study can be considered as a hydrodynamic liquid accompanied with the viscoelastic transition related to the structural relaxation in a sound velocity.

IV. CONCLUSION

For the investigation of the anisotropy in the collective dynamics of LC, IXS experiments have been conducted for two major directions ($Q \perp n$ and $Q \parallel n$) of the LC phase and the liquid phase of PYP8O8. The anisotropies observed in IXS measurements were compared with those measured by TWA and BLS [7]. It is shown that the hydrodynamic sound velocity at Q region (i) evolves to higher sound velocity at Q region (ii). This transition can be considered as a structural relaxation process (viscoelastic transition), where the LC system behaves as hydrodynamiclike Q region (i) and solidlike in Q regions (ii) and (iii). Although the anisotropy in sound velocity was observed in the gigahertz region with BLS measurement, the Q dependency of sound velocity in the terahertz region [Q regions (ii) and (iii)] is almost isotropic between two directions of a LC system. However, the FWHM of the inelastic peak has an anisotropy and it follows the hydrodynamic behavior of Q^2 dependency even in Q region (ii).

We observed different characteristics of phonon propagation in the LC system for sound velocity and sound attenuation. From the experimental observation, LC can be considered as the liquid having hydrodynamic fluid even at the terahertz region with isotropic viscoelastic transition. In the case of the LC system, the anisotropy of the collective dynamics in the terahertz region is more in the viscosity feature than in the elastic feature of the system.

ACKNOWLEDGMENTS

We wish to acknowledge JST CREST (Grant No. JP-MJCR19I3) and KAKENHI (Grants No. 22K14200 and No. 22H02137) for their financial support. The authors would like to thank the Tokyo Institute of Technology, Open Facility Centre, Design and Production Division, Ookayama Plant for their advice on chamber machining and production. M.R. and J.M. thank Dr. Alfred Baron for expert advice about the model for the analysis of IXS spectra. The IXS experiments were performed at the BL35XU of SPring-8 with the approval of the Japan Synchrotron Radiation Research Institute (JASRI) (Proposals No. 2019A1596, No. 2019B1531, No. 2022B1105, and No. 2022B1553).

APPENDIX A: THE STRUCTURAL MODEL OF LC SYSTEM

Figure 8 shows the static structure model of the LC system employed in this study and the corresponding structural parameters. We have assumed rodlike molecules aligned along one direction. There are characteristic distances between

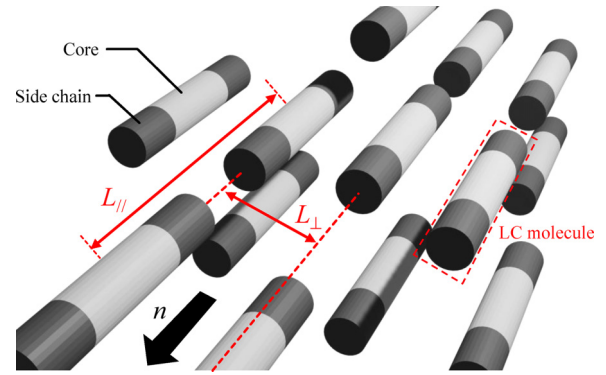


FIG. 8. The schematic view of the aligned LC model and the characteristic length of the structure used in the text.

molecules and they are different along the $\parallel n$ and $\perp n$ directions. Note that Fig. 8 does not include the effect of order parameter f and as discussed in the main text, the degree of orientation is not perfect as depicted in Fig. 8 in the real sample.

APPENDIX B: THE PLOT OF Q DEPENDENCY OF HWHM OF INELASTIC PEAK (γ_1) IN LOGARITHMIC SCALE

Figure 9 shows the dispersion of linewidth in logarithmic scale (corresponding to Fig. 6 in the main text) to indicate Q^2 dependency of Γ_1 .

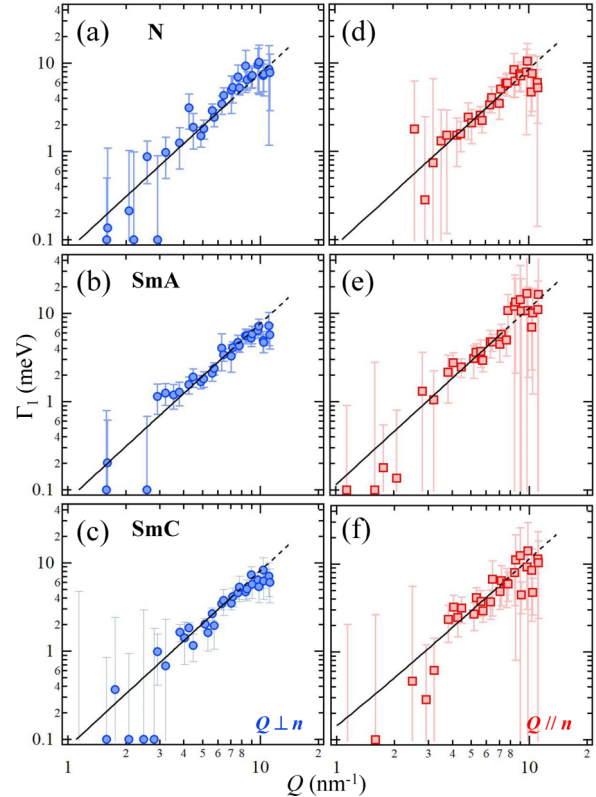


FIG. 9. The Q dependency of the HWHM of inelastic peak (Γ_1) of PYP8O8 along the molecular axis ($Q \parallel n$) (a)–(c) and along the perpendicular direction to the molecular axis ($Q \perp n$) (d)–(f) in logarithmic scale.

- [1] A. S. Henry and G. Chen, Spectral phonon transport properties of silicon based on molecular dynamics simulations and lattice dynamics, *J. Comput. Theor. Nanosci.* **5**, 141 (2008).
- [2] R. E. Newnham, *Properties of Materials: Anisotropy, Symmetry, Structure* (Oxford Academic, Oxford, 2004).
- [3] M. Ryu, H. Takezoe, O. Haba, K. Yonetake, and J. Morikawa, Photo-controllable thermal diffusivity and thermal conductivity driven by the orientation change of nematic liquid crystal with azo-dendrimers, *Appl. Phys. Lett.* **107**, 221901 (2015).
- [4] W. Urbach, H. Hervet, and F. Rondelez, Thermal diffusivity measurements in nematic and smectic phases by forced Rayleigh light scattering, *Mol. Cryst. Liq. Cryst.* **46**, 209 (1978).
- [5] M. Marinelli, F. Mercuri, U. Zammit, and F. Scudieri, Thermal conductivity and thermal diffusivity of the cyanobiphenyl (*n*Cb) homologous series, *Phys. Rev. E* **58**, 5860 (1998).
- [6] X. Xie, K. Yang, D. Li, T.-H. Tsai, J. Shin, P. V. Braun, and D. G. Cahill, High and low thermal conductivity of amorphous macromolecules, *Phys. Rev. B* **95**, 035406 (2017).
- [7] M. Ryu, Y. Cang, Z. Wang, G. Fytas, and J. Morikawa, Temperature-dependent thermoelastic anisotropy of the phenyl pyrimidine liquid crystal, *J. Phys. Chem. C* **123**, 17148 (2019).
- [8] Y. Cang, J. Liu, M. Ryu, B. Graczykowski, J. Morikawa, S. Yang, and G. Fytas, On the origin of elasticity and heat conduction anisotropy of liquid crystal elastomers at gigahertz frequencies, *Nat. Commun.* **13**, 5248 (2022).
- [9] G. Bradberry and C. Clarke, Temperature dependence and asymmetry of the hypersound velocity in cyanobiphenyl liquid crystals, *Phys. Lett. A* **95**, 305 (1983).
- [10] R. Sasaki, Y. Takahashi, Y. Hayashi, and S. Kawauchi, Atomistic mechanism of anisotropic heat conduction in the liquid crystal 4-heptyl-4'-cyanobiphenyl: All-atom molecular dynamics, *J. Phys. Chem. B* **124**, 881 (2020).
- [11] K. Yano, K. Yoshida, K. Kamazawa, H. Uchiyama, S. Tsutsui, A. Q. Baron, Y. Fukushima, and T. Yamaguchi, Investigation of collective dynamics of solvent molecules in nanofluids by inelastic x-ray scattering, *J. Mol. Liq.* **248**, 468 (2017).
- [12] D. Bolmatov, D. Soloviov, D. Zav'yalov, L. Sharpnack, D. M. Agra-Kooijman, S. Kumar, J. Zhang, M. Liu, and J. Katsaras, Anomalous nanoscale optoacoustic phonon mixing in nematic mesogens, *J. Phys. Chem. Lett.* **9**, 2546 (2018).
- [13] D. Soloviov, Y. Q. Cai, D. Bolmatov, A. Suvorov, K. Zhernenkov, D. Zav'yalov, A. Bosak, H. Uchiyama, and M. Zhernenkov, Functional lipid pairs as building blocks of phase-separated membranes, *Proc. Natl. Acad. Sci. USA* **117**, 4749 (2020).
- [14] B. Fåk and B. Dorner, Phonon line shapes and excitation energies, *Phys. B: Condens. Matter* **234–236**, 1107 (1997).
- [15] C. Masciovecchio, G. Ruocco, F. Sette, M. Krisch, R. Verbeni, U. Bergmann, and M. Soltwisch, Observation of large momentum phononlike modes in glasses, *Phys. Rev. Lett.* **76**, 3356 (1996).
- [16] H. Sinn, E. E. Alp, A. Alatas, J. Barraza, G. Bortel, E. Burkel, D. Shu, W. Sturhahn, J. Sutter, T. Toellner, and J. Zhao, An inelastic x-ray spectrometer with 2.2 meV energy resolution, *Nucl. Instrum. Methods Phys. Res., Sect. A* **467–468**, 1545 (2001).
- [17] V. K. Malinovsky, V. N. Novikov, P. P. Parshin, A. P. Sokolov, and M. G. Zemlyano, Universal form of the low-energy (2 to 10 meV) vibrational spectrum of glasses, *Europhys. Lett.* **11**, 43 (1990).
- [18] F. Bencivenga and A. Cunsolo, The dispersive behavior of collective excitations in fluids: An experimental test for the generalized collective modes theory, *J. Chem. Phys.* **136**, 114508 (2012).
- [19] R. Kiefer and G. Baur, Density studies on various smectic liquid crystals, *Liq. Cryst.* **7**, 815 (1990).
- [20] G. Heppke, D. Lotzsch, and N. K. Sharma, Liquid crystalline 2-[4-(2-chloroalkanoxy)-phenyl]-5-(4-*n*-hexyloxyphenyl)-pyrimidines—New ferroelectric compounds exhibiting interesting polymorphism, *Mol. Cryst. Liq. Cryst.* **241**, 275 (1994).
- [21] S. Inui, S. Kawano, M. S. H. Iwane, Y. Takanishi, K. Hiraoka, Y. Ouchi, H. Takezoe, and A. Fukuda, First order paraelectric-antiferroelectric phase transition in a chiral smectic liquid crystal of a fluorine containing phenyl pyrimidine derivative, *Jpn. J. Appl. Phys.* **29**, L987 (1990).
- [22] D. Forster, T. C. Lubensky, P. C. Martin, J. Swift, and P. S. Pershan, Hydrodynamics of liquid crystals, *Phys. Rev. Lett.* **26**, 1016 (1971).